Available online at www.sciencedirect.com

ScienceDirect

Geochimica et Cosmochimica Acta 228 (2018) 81–94

Geochimica et Cosmochimica Acta

www.elsevier.com/locate/gca

A new type of highly-vaporized microtektite from the Transantarctic Mountains

M. Van Ginneken [a,b,1,2,*], M.J. Genge [a], R.P. Harvey [c]

[a] IARC, Department of Earth Science and Engineering, Imperial College London, Exhibition Road, London SW7 2AZ, UK
[b] Department of Earth Science, The Natural History Museum, London SW7 2BT, UK
[c] Department of Geological Sciences, 112 A. W. Smith Building, Case Western Reserve University, Cleveland, OH 44106-7216, USA

Received 9 June 2017; accepted in revised form 23 February 2018; available online 6 March 2018

Abstract

We report on the discovery of microtektites (microscopic impact glass spherules) in a glacial moraine near Larkman Nunatak in the Transantarctic Mountains, Antarctica. The microtektites were identified based on their physical and chemical properties. Major and trace element compositions of the particles suggest that they may be related to the Australasian strewn field. This would further extend the current strewn field ~800 km southward. Depletion in volatiles and enrichment in refractory elements in Larkman Nunatak microtektites fit the volatilization trend defined by Australasian microtektites, suggesting that they may represent a new highly vapor fractionated end-member thereof. This observation is supported by their low vesicularity and absence of mineral inclusions. This discovery has significant implications for the formation of microtektites (i.e. their evolution with respect to the distance from the source crater). Finally, the discovery of potentially old (i.e. 0.8 Ma) microtektites in moraine has implications for the stability of the East Antarctic Ice Sheet in the Larkman Nunatak area over the last ~1 Ma and, as a consequence, the high efficiency of such moraines as traps for other extraterrestrial materials (e.g. micrometeorites and meteoritic ablation debris).

Keywords: Microtektite; Australasian; Impact cratering; Transantarctic Mountains; East Antarctic Ice Sheet; Micrometeorites

1. INTRODUCTION

Microtektites are the microscopic counterpart of tektites, which are glass objects resulting from the melting and vaporization of the Earth's crust during hypervelocity impacts of extraterrestrial bodies (Glass, 1990; Koeberl, 1994; Artemieva, 2008; Glass and Simonson, 2013). They are usually scattered over regions distal to impact craters called strewn fields (e.g., Glass and Simonson, 2013). To date, four major strewn fields have been discovered on the Earth's surface (i.e. Australasian, Central European, Ivory Coast and North America; Glass and Simonson, 2013). The Australasian strewn field is characterized by its large geographical extent that is at least an order of magnitude greater than that of other strewn fields (i.e. 14,000 km; Fig. 1; Folco et al., 2008; Glass and Simonson, 2013) and its relatively young age (~0.8 Ma; Izett and Obradovich, 1992). Despite its recent formation, the source crater of this strewn field has yet to be found. Several studies based on the distribution and/or geochemical properties of tektites and microtektites suggest that the source crater may be located in South East Asia, and probably in Vietnam (e.g., Glass and Pizzuto, 1994; Lee and Wei, 2000;

* Corresponding author at: IARC, Department of Earth Science and Engineering, Imperial College London, Exhibition Road, London SW7 2AZ, UK.
E-mail address: Matthias.Van.Ginneken@ulb.ac.be (M. Van Ginneken).
[1] Current address: Department of Analytical, Environmental and Geo-Chemistry, Vrije Universiteit Brussel, Pleinlaan 2, 1050 Brussel, Belgium.
[2] Current address: Laboratoire G-Time, Université Libre de Bruxelles, Franklin Rooseveltlaan 50, 1050 Brussel, Belgium.

https://doi.org/10.1016/j.gca.2018.02.041
0016-7037/

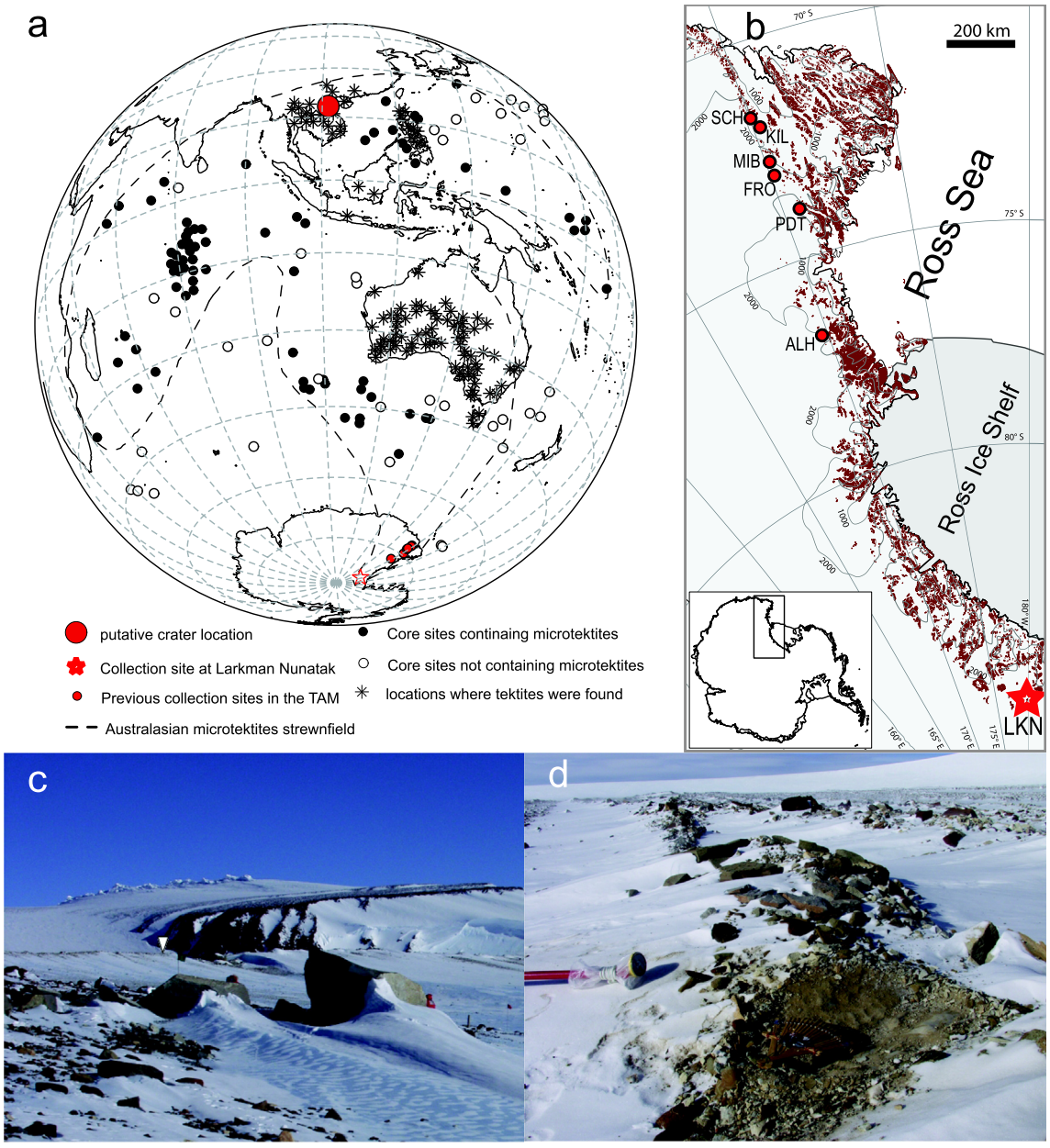

Fig. 1. Sampling location of Larkman Nunatak microtektites. (a) Sketch map showing the sampling sites of Australasian microtektites and the current extension of the Australasian strewn field. (b) Regional map showing the locations where microtektites were found in the Transantarctic Mountains. (c) Panoramic view of Larkman Nunatak. Arrowed is the sampling area where glacial moraine was collected. (c) Detail of the sampling area.

Ma et al., 2004; Glass and Koeberl, 2006; Prasad et al., 2007; Folco et al., 2010a, Folco et al., 2016).

Australasian microtektites have been found in deep sea sediments of the Indian and Pacific Ocean (hereafter AUS/DSS; e.g., Prasad and Sudhakar, 1999; Glass et al., 2004) and more recently on top of nunataks of the Transantarctic Mountains, Victoria Land, Antarctica (hereafter AUS/TAM; Folco et al., 2008; Folco et al., 2009). The current southernmost limit of the strewn field has been established after the discovery of Australasian microtektites in glacial sediment collected at a low relief crest next to Allan Hills, Victoria Land, Antarctica, which is situated approximately 11,000 km away from the hypothetical source crater location (Folco et al., 2016).

Here we describe the discovery of microtektites in glacial moraine collected next to the Larkman Nunatak in the Transantarctic Mountains, Antarctica. We first describe their geochemical affinities with Australasian microtektites (both AUS/DSS and AUS/TAM), suggesting that these two materials are paired. Subsequently, we will show that the microtektites from Larkman Nunatak expand the volatilization trends observed within AUS/DSS and

AUS/TAM and, as a result, represent a new highly volatile depleted end-members for these trends.

2. SAMPLE AND METHODS

2.1. Samples

The samples were recovered in 2006 by one of us (MG) from a glacial moraine near Larkman Nunatak (hereafter LKN; 85° 46′S, 179° 23′ E), along with hundreds of micrometeorites (Fig. 1b, c and d; Van Ginneken et al., 2016). At the time of recovery, the moraine was covered by a 4 cm thick snow cover. The moraine is oriented East–West and extends ca. 1.5 km with a width of 700 m. It rises up to 30 m above the surrounding meteorite-rich blue ice and it is separated from the nunatak by a depression of up to 500 m wide. Samples were collected from the southern edge of a boulder ridge approximately 40 m into the moraine and located approximately half way through the moraine along an East–West traverse. Detailed information on the bedrock and lithology of the moraine is provided in Van Ginneken et al. (2016).

In the laboratory 250 g of moraine samples were first washed in water and hydrogen peroxide to remove evaporite incrustations that prevented the identification of microtektites. They were subsequently dried and size separated using 106, 250, 425, 850 and 2000 μm sieves. Glacial sediment >2000 μm in size was not included. Fifty-two microtektites-like particles >106 μm in size were subsequently hand-picked from the sieved material under a stereomicroscope. Samples were identified on the basis of their spherical shape, pale yellow color and transparency.

2.2. Petrography and major element analyses

The microtektites were first mounted on clear adhesive tape and observed using a LEO 1455 environmental Scanning Electron Microscope (SEM) at the Imaging and Analysis Centre (IAC) of the National History Museum (NHM), London, United Kingdom, in order to gather information on their external features. Subsequently, a set of 13 microtektites were embedded in epoxy, sectioned, polished and carbon coated at the NHM. The remaining 39 particles were consumed in unsuccessful Ar-Ar analyses.

The major element composition of the microtektites was determined using a Cameca SX100 electron microprobe at the IAC that is equipped with five wavelength dispersive spectrometers. Bulk compositions were calculated by averaging four point analyses for each particle. A defocused beam ~10 μm in size was used in order to reduce the loss of volatile elements. Operating conditions were an accelerating voltage of 20 kV, a 20.0 nA beam current. A number of synthetic and natural standards were used for instrumental calibration. Standards include but were not limited to: forsterite (Mg_2SiO_4) (San Carlos olivine) for calibration of Mg, hematite (Fe_2O_3) for Fe calibration, wollastonite ($CaSiO_3$) for Si and Ca calibration and corundum (Al_2O_3) for Al calibration. The built-in PAP-algorithm (e.g., Pouchou and Pichoir, 1991) was used for correction. The detection limits (in wt.%) are: Si = 0.01; Ti = 0.03; Al = 0.01; Fe = 0.03; Mn = 0.03; Mg = 0.01; Ca = 0.03; Na = 0.03; K = 0.04.

2.3. Trace element analyses

Trace element compositions of 11 microtektites were determined by Laser Ablation Inductively Coupled Plasma Mass Spectrometry at the IAC. The instrument was a Agilent 7500 ICP quadrupole mass spectrometer coupled with a ESI NWR193 ArF excimer laser source. The laser was operated at a repetition rate of 10 Hz, the spot size was 45 μm, and the energy at 3.2 mW. Signals for the analytical masses reported in Table 3 were acquired in peak hopping mode with 10 ms dwell time. Analyses consisted of the acquisition of 30 s background signal and one minute ablation signal. Data reduction was performed with the software LamTrace (Jackson, 2008). NIST SRM 612 (Hinton, 1999) and ^{43}Ca were adopted as external and internal standards, respectively. Precision and accuracy were assessed via repeated analysis of BCR-2 g, resulting better than 7% and ±10%, respectively, at the mg/g concentration level. Mean detection limits at 45 μm spot size for the quadrupole instrument are reported in Table 3.

3. RESULTS

3.1. Overall description

The 52 samples are transparent glass spherules (Fig. 2). The color of all spherules is pale yellow and in all cases their shape has a high degree of sphericity. Only one microtektite exhibits a bubble ~10 μm in diameter in its interior (Fig. 2c). The surface of most particles is smooth and featureless (Fig. 3a), but 8% of the particles show weathering pits (Fig. 3b) identical to those observed on the surfaces of V-type (i.e. glassy) cosmic spherules extracted from the same glacial moraine (Van Ginneken et al., 2016). The particles also lack microscopic impact craters reported on an Australasian microtektite (Prasad and Sudhakar, 1996). The SEM backscattered images of sectioned samples show constant Z-contrast, suggesting that their chemical compositions are homogeneous (Fig. 3c and d).

The size of the samples varies between 107 and 388 μm. The size distribution of the particles (Fig. 4) is normal, except for a depletion at around 200 μm that is probably a statistical bias owing to low count statistics. Size fractions of glacial moraine larger than 400 μm were searched for microtektites but none were found, suggesting this is their maximum size limit in the deposit.

3.2. Bulk chemistry

The major element bulk compositions of 13 samples is reported in Table 1. Major element concentrations vary from one particle to another, but compositional trends are observed. Most major oxides are inversely correlated to SiO_2 (Fig. 5) that shows concentrations ranging from

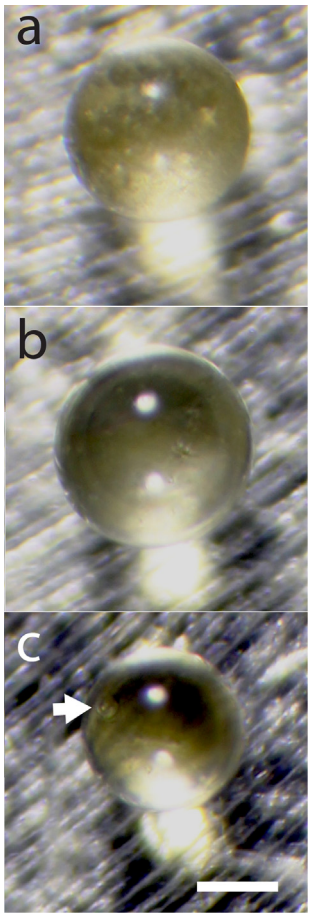

Fig. 2. Stereomicrograph of three Larkman Nunatak microtektites. The scalebar is 100 μm. A vesicle is arrowed in (c).

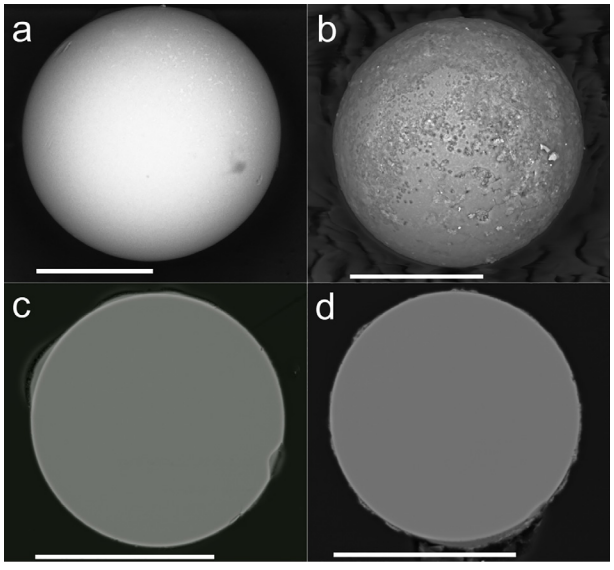

Fig. 3. Scanning electron microscope backscattered images of microtektites from Larkman Nunatak. (a) Details of the smooth surface of a microtektite. (b) The rugged surface of a microtektite showing weathering pits typical of chemical alteration in the glacial moraine. (c and d) Polished sections of microtektites showing the apparent chemical homogeneity of the samples.

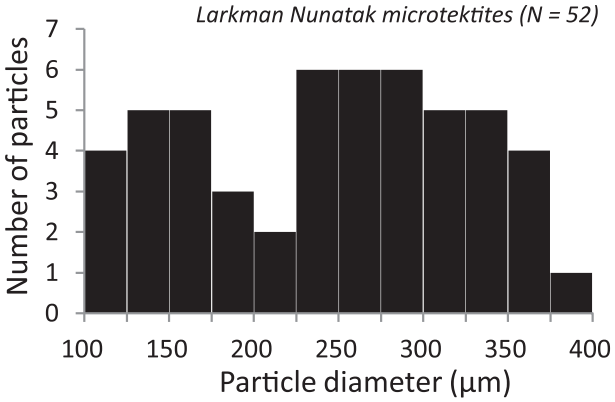

Fig. 4. Size (mean diameter) distribution of the 52 Larkman Nunatak microtektites collected so far. microtektites. The microtektites were collected in the 106–2000 μm size fraction, so the upper limit of this diagram is the actual upper size limit of the microtektites collected. On the other hand, the lower limit is mainly due to the smallest mesh size used for sieving and may not represent the lower size limit of the microtektites.

43.7 to 64.5 wt%. MgO, Al_2O_3, CaO and TiO_2 range from 4.36 to 11.9, 18.9 to 35.1, 3.27 to 9.35 and 1.04 to 1.79 wt %, respectively. Conversely, FeO is positively correlated with SiO_2 and ranges from 1.06 to 3.95 wt%. The Na_2O and K_2O contents also slightly increase with SiO_2 and range from 0.07 to 0.39 and 0.10 to 0.81 wt%, respectively.

When compared to known microtektites populations classified according to Glass et al. (2004), only four samples have major element compositions overlapping those of normal AUS/DSS and AUS/TAM microtektites (Fig. 5; i.e. "normal microtektites" have major oxide compositions similar to Australasian tektites; Glass et al., 2004). The nine remaining particles show silica contents significantly lower than that of normal AUS/DSS and AUS/TAM microtektites. Conversely, an enrichment in Al_2O_3, TiO_2 and CaO is observed. About half of the particles show MgO contents that overlap normal AUS/DSS and AUS/TAM microtektites compositional fields, the rest being enriched. FeO is depleted in only four samples. The low Na_2O content overlaps that of normal AUS/TAM microtektites in all particles except for particle #LK06-1159, in which it is significantly depleted at 0.07 wt%. Eight samples show K_2O that is lower than microtektites from other collections. Our samples show major element compositions that plot between the compositional field of normal AUS/DSS and AUS/TAM microtektites and a high-Al AUS/DSS microtektite (Glass et al., 2004). Two similar high-Al AUS/TAM microtektites have major element composition overlapping that of our samples (Folco et al., 2016). Comparison with differentiated cosmic spherules (i.e. having non-chondritic chemical composition) show that our samples plot in distinct compositional fields, especially when considering FeO and Al_2O_3 that show systematically higher and lower values, respectively (Fig. 5).

Table 2 lists the trace element compositions of 11 samples that was determined by LA-ICP-MS. The major and trace element compositions of our samples,

Table 1
Major element bulk compositions (in oxide wt%) of microtektites from Larkman Nunatak. Bulk compositions were determined using EPMA and by averaging four defocused beam (typically 10 μm in diameter) point analyses in each sample.

Sample	Ø (μm)	SiO_2	TiO_2	Al_2O_3	FeO[a]	MnO	MgO	CaO	Na_2O	K_2O	Total
LK06-1149	142	53.3	1.39	24.4	2.91	0.08	9.83	6.88	0.19	0.21	99.21
LK06-1150	135	64.5	1.04	18.9	3.95	0.10	6.40	3.27	0.39	0.79	99.27
LK06-1151	154	52.9	1.17	24.1	3.13	0.08	10.61	6.49	0.15	0.18	98.84
LK06-1152	162	60.6	1.19	21.7	3.78	0.10	5.95	5.00	0.31	0.57	99.25
LK06-1153	106	49.9	1.68	32.3	2.28	0.05	5.92	6.52	0.25	0.37	99.30
LK06-1154	137	62.1	1.20	22.2	3.48	0.08	4.36	4.42	0.39	0.81	99.07
LK06-1155	112	51.4	1.21	25.1	3.36	0.08	11.88	6.06	0.25	0.29	99.66
LK06-1156	124	49.6	1.38	27.5	3.68	0.08	9.40	6.97	0.25	0.28	99.16
LK06-1157	153	56.9	1.32	25.5	3.22	0.09	5.69	5.33	0.30	0.54	98.93
LK06-1158	142	63.0	1.08	20.4	3.81	0.09	4.80	4.83	0.37	0.75	99.10
LK06-1159	127	43.7	1.79	35.1	1.06	0.03	7.80	9.35	0.07	0.10	99.01
LK06-1160	170	46.8	1.52	29.9	2.62	0.06	11.07	7.09	0.14	0.19	99.41
LK06-1161	166	49.4	1.53	32.8	2.48	0.07	5.17	7.28	0.16	0.25	99.21

[a] All Fe as FeO.

AUS/DSS and AUS/TAM microtektites and of the Upper Continental Crust (UCC) were normalized to CI chondrites (Fig. 6). The geochemical patterns of the samples are broadly similar to those of the UCC and AUS/TAM and AUS/TAM microtektites. However, their chemical composition exhibit variations from the UCC common to AUS/DSS and AUS/TAM microtektites. Refractory elements Sc, Cr, Y, Zr, REE, Hf and Th are consistently enriched with respect to the UCC, whereas other refractory and some moderately volatile elements Li, Be, Mg, Al, Si, Fe, Ca, Mn, Nb, Ba and Ta plot close to the UCC, except for Fe in particle #LK06-1159 that is depleted. Conversely, volatile to highly volatile elements Na, K, Zn, Rb, Sr and Cs are significantly depleted compared to the UCC.

Although plotting in the same compositional fields, contents in volatile element Rb (10 ± 7 ppm), Cs (1 ± 0 ppm) and Zn (1 ± 0 ppm) of the samples exhibit values in the lower range of normal AUS/TAM (41 ± 15, 2 ± 1, 3 ± 2 ppm, respectively) and AUS/DSS (88 ± 52, 5 ± 3, 14 ± 1 2 ppm, respectively) microtektites (Fig. 8). Conversely, refractory elements like La (74 ± 13 ppm), Hf (12 ± 3 pp m) and Th (28 ± 5 ppm) exhibit concentrations in the samples in the higher range of normal AUS/TAM (53 ± 8, 8 ± 1, 19 ± 2 ppm, respectively) and AUS/DSS (48 ± 9, 9 ± 2, 17 ± 4 ppm, respectively) microtektites. Rare Earth Elements are enriched compared to normal AUS/DSS and AUS/TAM microtektites, as evidenced in Fig. 6. Similar depletions and enrichments are observed when comparing to high-Mg AUS/DSS and AUS/TAM microtektites. Our samples show patterns matching those of High-Al AUS/DSS and AUS/TAM microtektites (Fig. 6). Only Zn and Rb are significantly depleted in LKN microtektites. Ni and Co contents are low in 9 samples, similarly to what is observed in AUS/TAM. However, microtektites #LK06-1155 and #LK06-1156 show significant enrichments in Ni and Co by a factor of ~5 compared to AUS/TAM microtektites. Values in Ni and Co in these two samples are consistent with those in normal AUS/DSS microtektites and high-Al AUS/DSS microtektites (Fig. 6).

4. DISCUSSION

4.1. A new southernmost extension to the Australasian microtektites strewn field

The glassy spherules collected in the glacial moraine near LKN are identified as microtektites on the basis of several criteria: (1) their pale-yellow color allows their distinction from V-type cosmic spherules found within the same sediment, which usually exhibit darker colors (Genge et al., 2008; Van Ginneken et al., 2016). Furthermore, this pale-yellow color is typical of normal AUS/DSS and AUS/TAM microtektites (Glass et al., 2004; Folco et al., 2009). However, V-type cosmic spherules exhibit a wide range of color and transparency (Genge et al., 2008), so this criterion should be used in addition with the following criteria; (2) Their major and trace element chemistry is broadly similar to that of the Upper Continental Crust (Taylor and McLennan, 1995), which is also typical of the microtektites from the main known strewn fields (Glass et al., 2004); (3) Their major element chemistry is clearly distinct from that of differentiated cosmic spherules (Taylor et al., 2007; Cordier et al., 2011; Cordier et al., 2012), which represent potential alternatives to microtektites as glassy micro-spherules exhibiting non-chondritic compositions; (4) The total alkali content ($Na_2O + K_2O$) of all samples is lower (0.18–1.20 wt%) than in volcanic glasses for a given silica content, and K_2O/Na_2O is always >1. These geochemical features are characteristic of tektitic material (Koeberl, 1990). All these criteria suggest that these glassy spherules recovered at LKN are indeed microtektites.

Pairing microtektites originating from different sampling locations based on their geochemistry alone can be challenging because of important chemical overlaps between populations originating from different strewn fields (Koeberl, 1990; Glass et al., 2004). The major element compositions of normal Australasian, Ivory Coast and North American microtektites, for example, overlap significantly (Fig. 5). However, normal AUS/TAM microtektites are

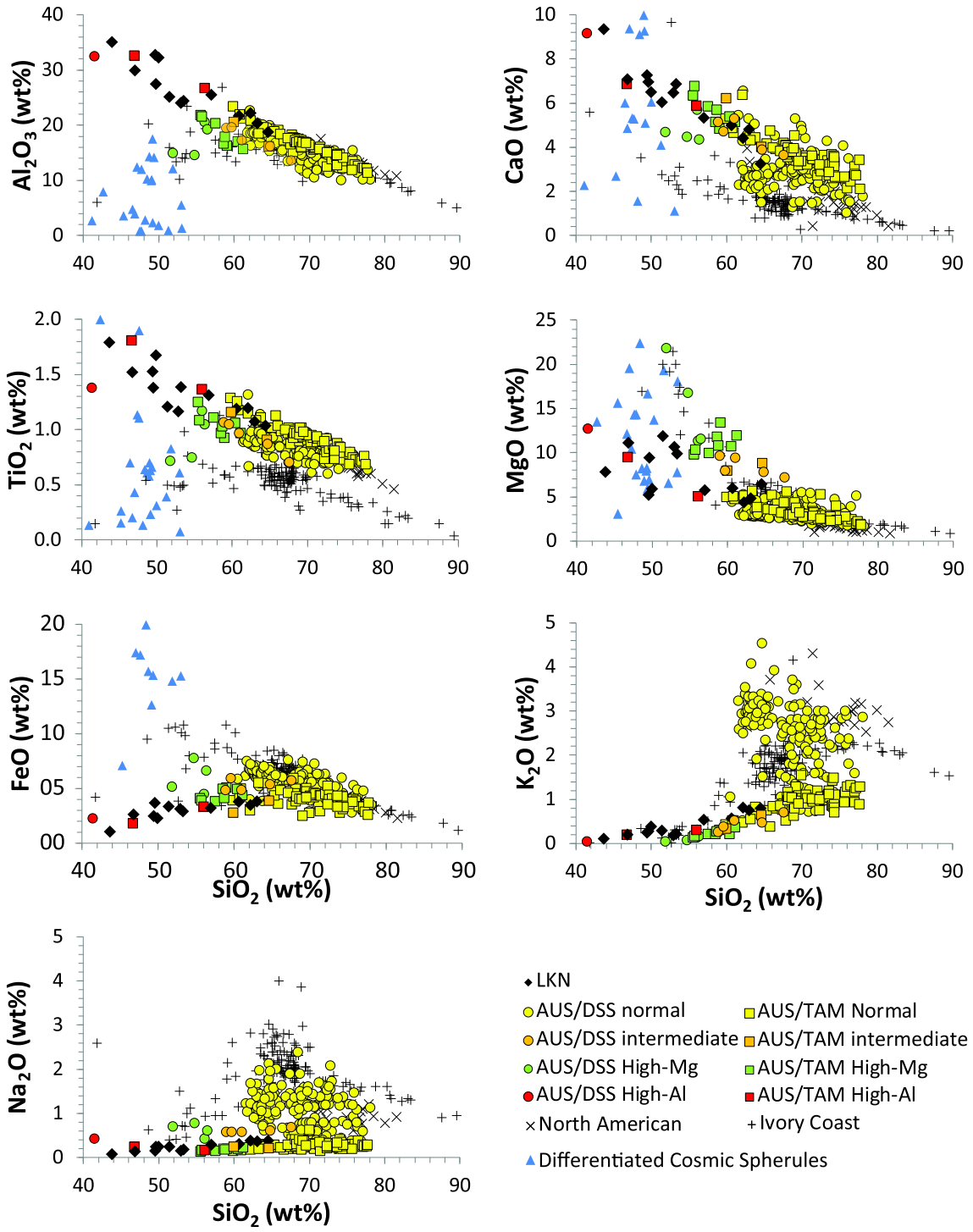

Fig. 5. Harker diagrams showing the major element composition against SiO_2 of Larkman Nunatak microtektites compared to literature data on microtektites (Glass et al., 2004; Folco et al. 2009, 2016) and achondritic V-type cosmic spherules (Taylor et al., 2007; Cordier et al., 2011; Cordier et al., 2012). All values are in wt%.

enriched in the refractory element Ca and depleted in alkali elements compared to normal AUS/DSS microtektites due to their more distal deposition relative to the hypothetical source crater and resulting increased volatilization (Folco et al., 2010a). Consequently, AUS/TAM microtektites plot in distinct compositional fields from Ivory Coast and North American microtektites while still overlapping those of AUS/DSS microtektites.

Out of 13 LKN microtektites, 9 have major element compositions plotting in-between the composition fields

Table 2
Trace element bulk compositions (μg/g) of microtektites from Larkman Nunatak determined by LA-ICP-MS.

Sample	LK06-1149	LK06-1150	LK06-1151	LK06-1152	LK06-1153	LK06-1154	LK06-1155	LK06-1156	LK06-1157	LK06-1158	LK06-1159
Li	20.4	28.6	17.3	32.0	36.1	31.4	23.7	27.7	32.5	29.9	19.9
Be	4.68	3.41	4.21	4.13	6.30	4.02	3.97	5.14	4.87	3.70	6.35
Sc	26.2	23.4	24.9	25.3	31.1	26.0	24.3	26.3	27.4	26.3	32.0
V	50.7	26.7	35.9	31.1	46.4	25.9	60.4	58.8	29.8	26.8	50.1
Cr	474	109	142	146	118	86.3	665	634	92.7	146	123
Co	3.42	3.2	1.62	2.84	1.19	2.2	8.83	10.2	1.65	3.57	0.64
Ni	10.7	1.69	1.56	3.3	2.82	3.45	58.6	68.3	1.77	2.87	4.91
Zn	1.1	0.59	0.77	0.61	0.79	0.76	1.23	1.18	0.84	0.64	0.97
Rb	4.05	18.6	3.25	12.5	5.28	20.3	6.49	6.27	10.4	17.4	2.31
Sr	334	212	353	274	344	244	317	391	294	264	461
Y	49.2	42.9	49.8	45.3	60.2	42.5	41.4	54.4	50.2	46.8	72.1
Zr	471	460	513	402	470	335	365	508	418	432	698
Nb	29.6	26	25.2	27.3	36.5	25.9	25.6	29.4	30.3	25.4	38.6
Cs	0.17	0.97	0.14	0.69	0.25	1.15	0.29	0.24	0.59	0.94	0.07
Ba	788	589	659	627	880	621	644	893	717	487	1000
La	71.4	62	75.7	64.6	89	61.6	70.2	81.5	73.3	62	103
Ce	127	111	101	123	162	119	107	136	130	108	154
Pr	16.1	13.8	16.1	14.6	20.2	13.7	14.7	18.5	16.3	12.8	22.4
Nd	59.1	51.5	62.6	54.9	75	53	59.7	68.6	61.8	51.7	86.8
Sm	11.4	10.2	12	10.6	14.2	10.2	11.3	13.7	12.4	10.3	17
Eu	2.37	1.87	2.28	2.04	2.73	2.01	2.26	2.68	2.29	1.95	3.3
Gd	9.82	8.36	9.94	9.01	12.6	9.07	8.98	11	10.5	9.26	14.5
Tb	1.48	1.29	1.48	1.39	1.86	1.35	1.35	1.65	1.61	1.39	2.19
Dy	9.05	7.66	8.76	8.51	11.2	7.87	8.09	9.94	9.53	8.7	13.1
Ho	1.78	1.57	1.85	1.71	2.25	1.58	1.55	2.01	1.9	1.76	2.74
Er	5.03	4.52	5.45	4.9	6.39	4.51	4.47	5.89	5.32	5.13	7.53
Tm	0.77	0.66	0.77	0.68	0.93	0.62	0.63	0.81	0.75	0.71	1.05
Yb	5.08	4.56	5.42	4.77	6.45	4.4	4.44	5.76	5.34	5.05	7.91
Lu	0.72	0.65	0.8	0.71	0.95	0.62	0.63	0.82	0.77	0.72	1.1
Hf	12.3	11.9	14.9	10.9	12.4	9.03	8.96	13.1	11	11.5	18.2
Ta	2.22	2.02	2.39	2.07	2.82	1.95	2.11	2.59	2.39	2.05	3.1
Pb	*b.d.l.*	*b.d.l.*	*b.d.l.*	*b.d.l.*	*b.d.l.*	*b.d.l.*	*b.d.l.*	*b.d.l.*	*b.d.l.*	*b.d.l.*	*b.d.l.*
Th	26	23	27.6	24.4	33.5	23	25.8	29.6	28.1	23.9	37.8
U	0.8	0.24	0.36	0.3	0.56	0.19	0.94	0.88	0.26	0.23	0.83

b.d.l. = below detection limit.

Table 3
Acquired analytical masses by LA-ICP-MS and mean detection limits (M.D.L.) at 45 μm spot size.

Element	Mass	M.D.L. (μg/g)	Element	Mass	M.D.L. (μg/g)	Element	Mass	M.D.L. (μg/g)
Li	7	0.068	Nb	93	0.010	Dy	163	0.021
Be	9	0.114	Mo	95	0.051	Ho	165	0.005
Sc	45	0.067	Cs	133	0.007	Er	167	0.025
V	51	0.023	Ba	137	0.057	Tm	169	0.005
Cr	53	0.441	La	139	0.006	Yb	173	0.032
Co	59	0.036	Ce	140	0.006	Lu	175	0.006
Ni	60	0.117	Pr	141	0.005	Hf	177	0.029
Zn	66	0.176	Nd	145	0.063	Ta	181	0.006
Rb	85	0.012	Sm	147	0.036	Pb	208	0.034
Sr	88	0.008	Eu	151	0.011	Th	232	0.007
Y	89	0.008	Gd	157	0.035	U	238	0.006
Zr	90	0.016	Tb	159	0.005			

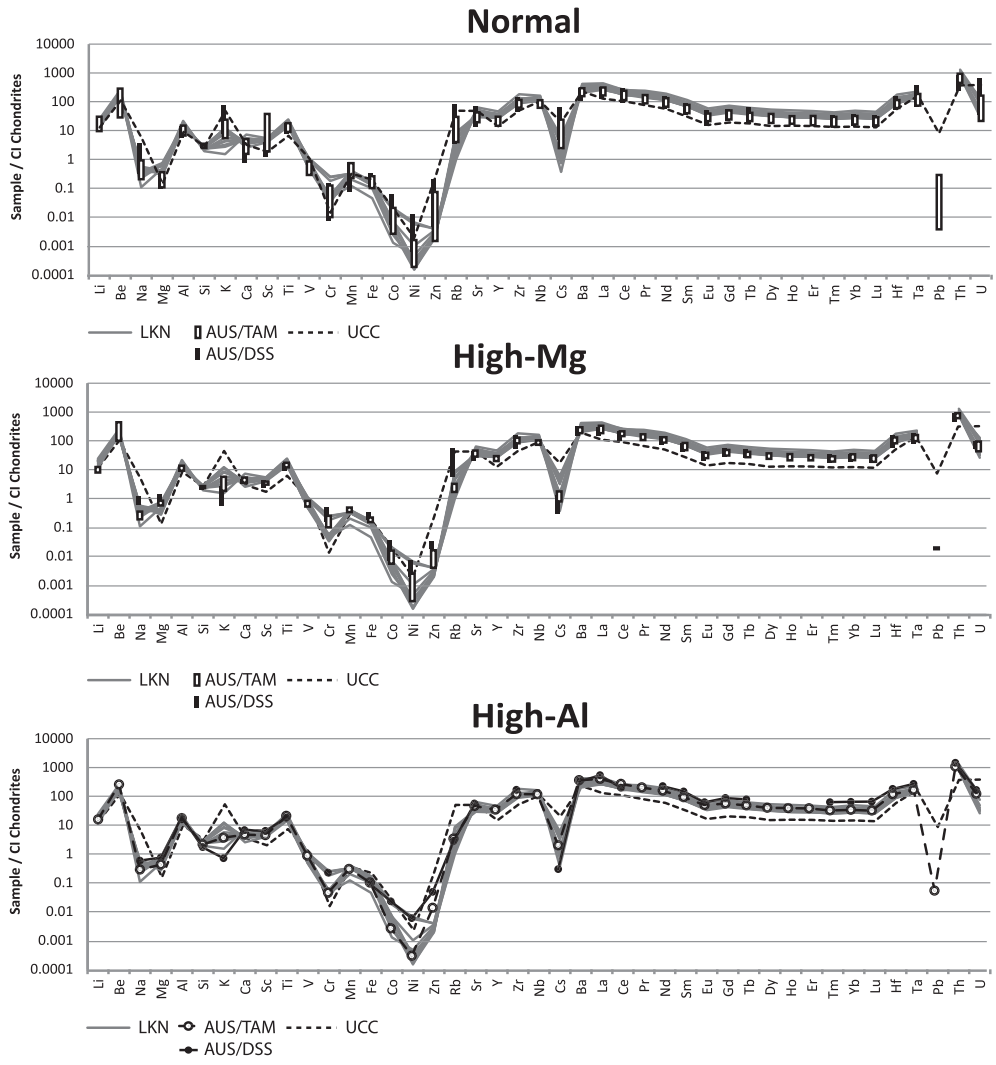

Fig. 6. Spider diagrams showing the major and trace element compositions of LKN and normal, high-Mg and high-Al of AUS and AUS/TAM microtektites (literature data from Taylor and McLennan, 1995; Koeberl et al., 1997; Glass et al., 2004; Folco et al., 2009; Folco et al., 2010a; Folco et al., 2016) normalized to CI chondrites (McDonough and Sun, 1995).

of normal and high-Al Australasian microtektites. However, three high-Al microtektites from both the AUS/DSS and AUS/TAM collections, which are severely enriched in refractory elements and depleted in volatiles, have major elements compositions within the same compositional field as LKN microtektites. Furthermore, the LKN microtektites seem to follow inverse chemical trends observed when plotting major elements (except alkalies) against SiO_2 of normal and high-Al AUS/DSS and AUS/TAM microtektites. Interestingly, for high-Al AUS/DSS and AUS/TAM microtektites, FeO follows a positive trend that is also observed in LKN microtektites. Although chemical trends are not obvious for alkali elements, LKN microtektites are particularly depleted in Na_2O and K_2O, similarly to AUS/TAM microtektites, albeit to a larger extent. Particle #LK06-1159, which exhibits the lowest SiO_2 content (i.e. 43.7 wt%), also has the lowest observed alkali content (0.07 and 0.10 wt% for Na_2O and K_2O, respectively). Lastly, the correlation of the refractory elements Al_2O_3 versus TiO_2 in LKN microtektites extend the linear trend previously observed in AUS/DSS and AUS/TAM microtektites (Folco et al., 2010a), which is clearly distinct from the trends observed for Ivory Coast and to a lower extent North American microtektites. Similar chemical trends are observed with trace elements in Harker diagrams of volatile against refractory elements (Fig. 8), with LKN microtektites showing affinities with high-Al Australasian microtektites mainly. More importantly, for identical volatile content, refractories La, Hf and Th in LKN microtektites overlap the compositional fields of AUS/DSS and AUS/TAM microtektites only.

The chemical similarity of LKN and Australasian microtektites suggest both were generated in the same impact event and have the same source crater. In particular, that LKN spherules lie on the extension of trends in alkali metals, refractory elements and iron observed only in Australasian microtektites is strong evidence for a genetic relationship. The LKN microtektite data testifies to a continued evolution of microtektite compositions, through the same chemical processes that control Australasian microtektites, making it very likely these represent distal ejecta from this impact event.

Until now Allan Hills has been the southernmost extension of the Australasian strewn field, however, the discovery of the LKN microtektites increases it by ~800 km, with a new maximum extension from the putative crater of ~12,000 km (Fig. 1a). This strengthens the hypothesis by Folco et al. (2016) that the distribution of Australasian microtektites in Antarctica is continental and not only limited to Northern Victoria Land. The maximum diameter of 388 μm of LKN spherules are also compatible with their identity as the southernmost extension to the Australasian strewn field. Although AUS/TAM microtektites are present in the same size range (Folco et al., 2009; Folco et al., 2016), their size distribution peaks at ~450 μm, with particles up to 560 μm in diameter in Allan Hills. This decrease in size from AUS/TAM to LKN microtektites further strengthens that the latter were deposited further away from the source location and represent the current maximum extension of the Australasian strewn field.

4.2. Expanding the volatilization trend of the Australasian microtektites

A common volatilization trend exists between AUS/DSS and AUS/TAM (Folco et al., 2010a) and is typified by the depletion in volatiles and enrichment in refractory elements with increasing distance from the hypothetical source crater. If the microtektites from Larkman Nunatak are indeed an extension of the Australasian strewn field, translating to a ~7% increase in distance from the hypothetical source crater, then it might be expected that the geochemistry of our microtektites will show a notable increase in volatilization with respect to AUS/DSS and AUS/TAM particles.

The most refractory major elements Ti and Al (Lodders, 2003) are not affected by volatilization during microtektite formation and thus, increased chemical fractionation due to volatilization at high temperature will not modify the TiO_2/Al_2O_3 ratio, which is representative of the target material. As a result, on a TiO_2 versus Al_2O_3 diagram, Australasian microtektite values plot along a linear trendline (e.g. Folco et al., 2010a). Fig. 7a shows that TiO_2/Al_2O_3 values of LKN microtektites plot along the same trendline of normal AUS/DSS and AUS/TAM and have a TiO_2/Al_2O_3 ratio of 0.052 (±0.003), similar to that of AUS/DSS and AUS/TAM of 0.056 (±0.005) (Folco

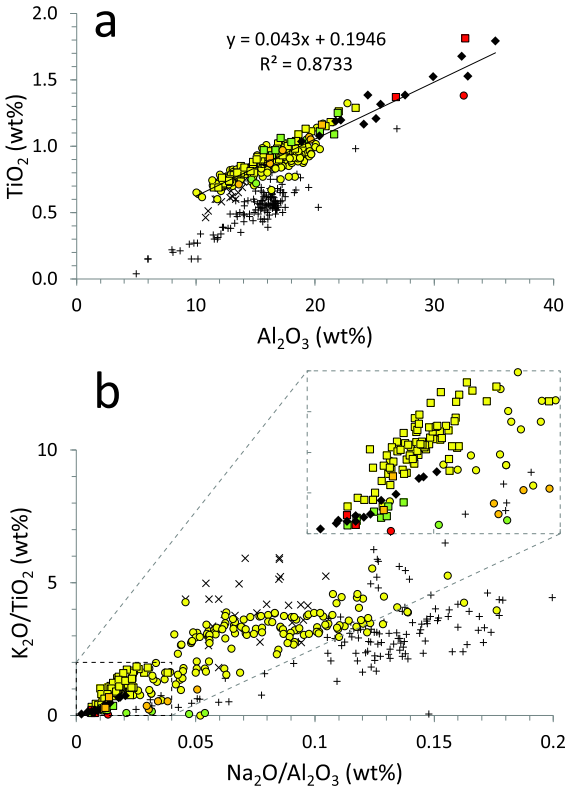

Fig. 7. Al_2O_3 vs. TiO_2 (a) and Na_2O/Al_2O_3 K_2O/TiO_2 (b) diagrams showing how Larkman Nunatak microtektites fit into the volatilization trend of AUS and AUS/TAM microtektites defined by refractory and volatile/refractory elements (Folco et al., 2010a). Symbols for LKN, AUS/DSS and AUS/TAM microtektites of Fig. 6 were used.

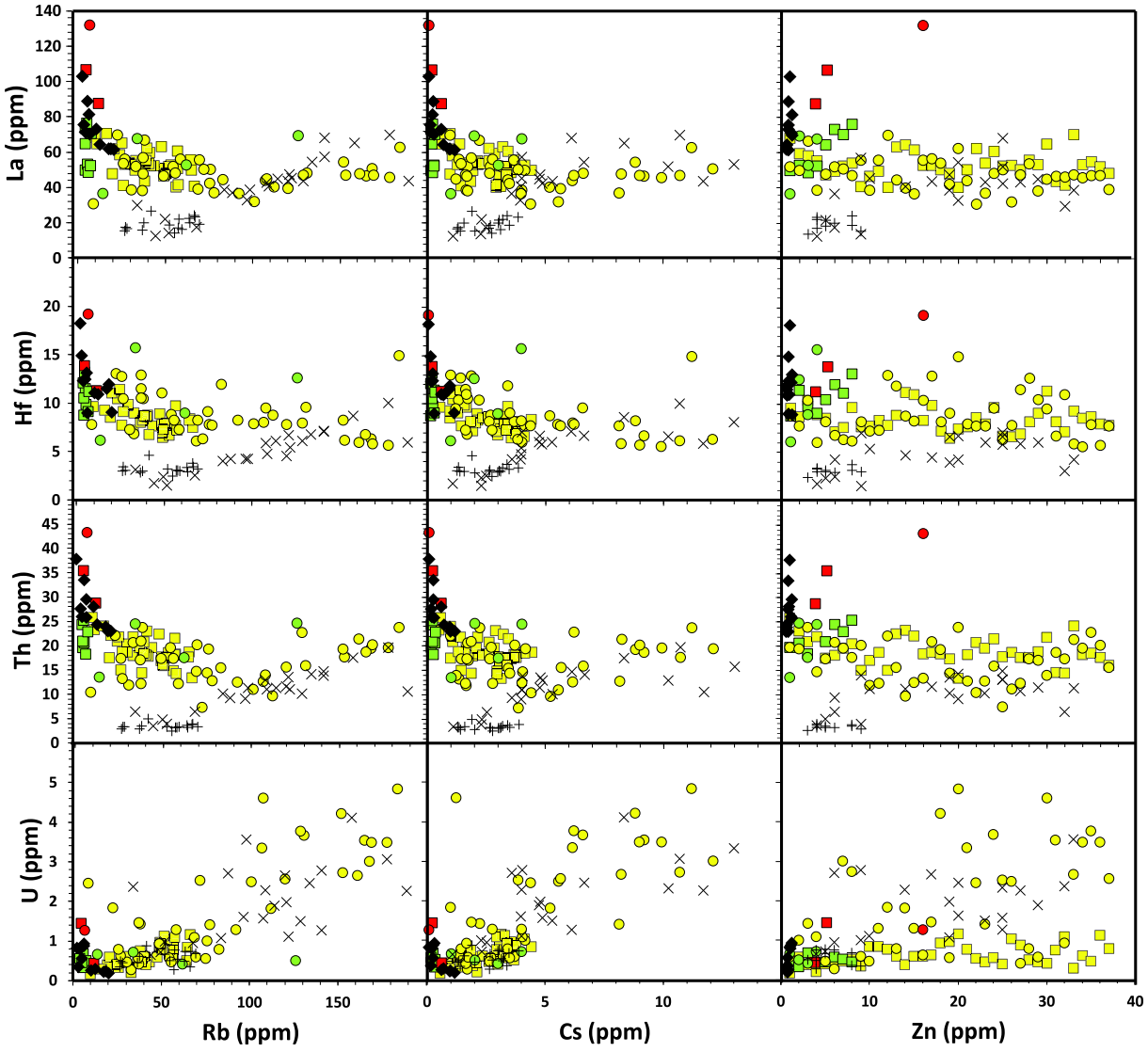

Fig. 8. Harker diagrams of volatile against refractory trace elements in Larkman Nunatak micrometeorites compared to data from the literature (Glass et al., 2004; Folco et al. 2009, 2016). All values are in μg/g. Symbols for LKN, AUS/DSS and AUS/TAM microtektites of Fig. 6 were used.

et al., 2016). More importantly, eight of our particles significantly extend the trendline towards more refractory compositions and in the compositional field previously defined by the high-Al AUS/DSS and AUS/TAM microtektites.

Additionally, the Ti and Al contents of LKN microtektites are inversely correlated to the content in alkali Na_2O and K_2O (Table 1 and Fig. 7b). Once again, LKN microtektites fall along the trend defined by AUS/DSS and AUS/TAM microtektites, with most of our particles plotting towards more volatile-poor contents. In particular, three particles exhibit the lowest values on the trendline, indicating that they are severely depleted in volatiles and enriched in refractory elements. This is consistent with the constant depletion in K_2O and Na_2O content with distance from the hypothetical source crater (Fig. 9), which is particularly pronounced in microtektites recovered in Antarctica. Thus, major elements support the contention that LKN microtektites are highly vapor fractionated and extend the common volatilization trend observed in Australasian microtektites.

Regarding trace elements, the LKN microtektites are depleted in volatile (Rb, Cs and Zn) and significantly enriched in refractory trace elements (La, Hf, Th) with respect to normal AUS/DSS and AUS/TAM microtektites (Fig. 8). The only exception being the refractory element U that is strongly enriched in most normal AUS/DSS microtektites. However, the range of U content in LKN particles is similar to that of normal AUS/TAM particles and strongly depleted compared to normal AUS/DSS and UCC (Figs. 6 and 8). Wasson et al. (1990) explained this depletion in U by volatilization, with possible enhancement by high pO_2 and preferential location of U in the reduced target's carbonaceous matter. Consistently with the major element discussed above, LKN microtektites plot in the

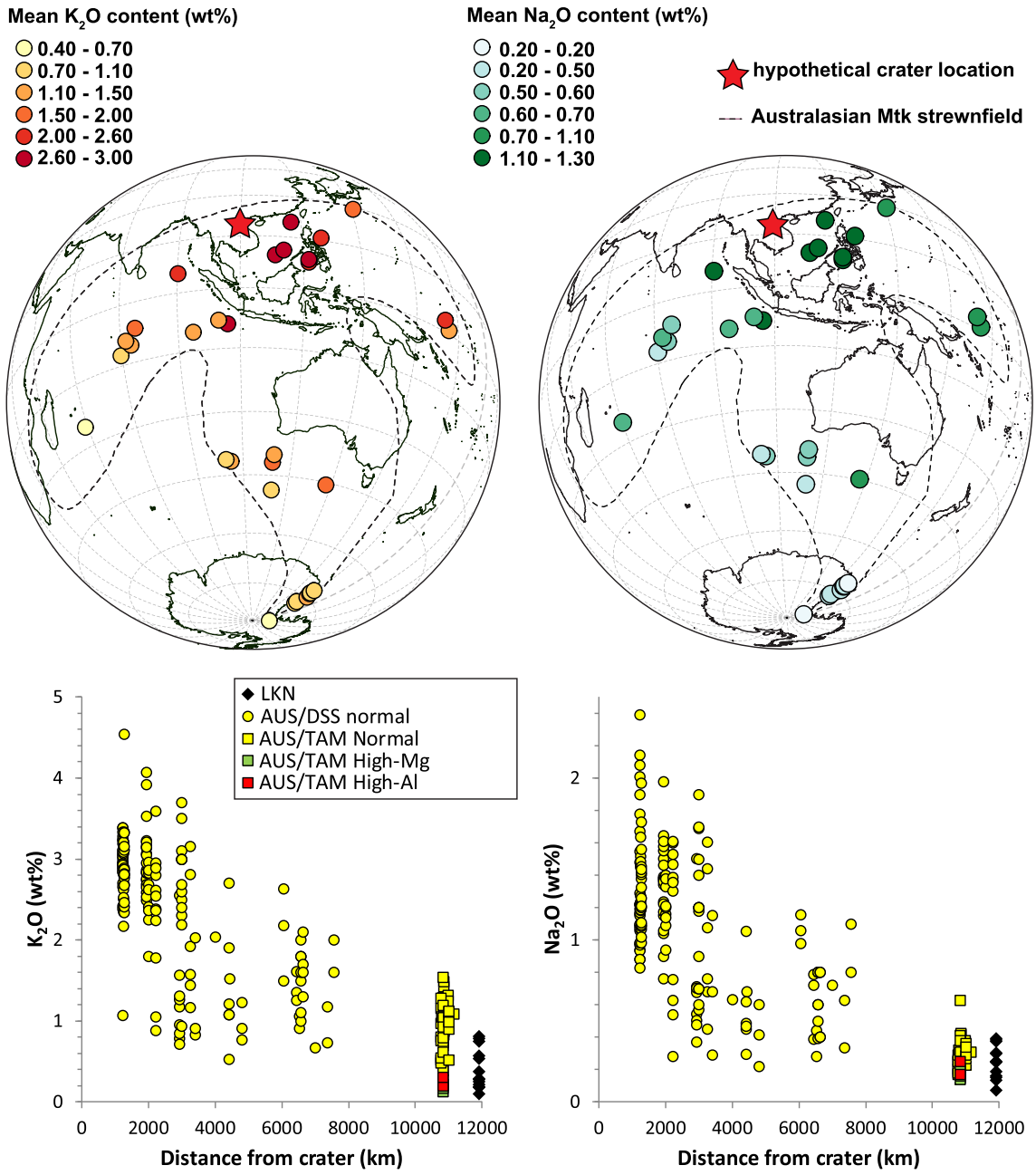

Fig. 9. Map and diagrams showing the evolution of K_2O and Na_2O in Larkman Nunatak and Australasian microtektites (both AUS and AUS/TAM; data from Cassidy et al. (1969), Glass et al. (2004), Glass and Koeberl (2006) and Folco et al. (2010a)) with distance from the hypothetical source crater in the Indochina region.

same compositional fields of high-Al AUS/DSS and AUS/TAM particles, except for Zn that is significantly higher in the latter and extremely depleted in LKN particles. Glass et al. (2004) argued that the high Zn content of high-Al AUS/DSS microtektite suggests that they may not represent a severely vapor fractionated end-member of the AUS microtektites, but rather a different population of microtektites, similarly to high-Mg "bottle green" microtektites (Glass, 1972; Folco et al., 2009). However, the severely depleted Zn content in LKN particles suggests that they may not be related to high-Al microtektites recovered closer to the hypothetical source crater and represent a new type of highly volatile depleted microtektites.

The occurrence of only one vesicle amongst recovered LKN microtektites (Fig. 2) indicates that vesicularity in this population is extremely low. This further supports a link with Australasian microtektites, as vesicularity has been observed to decrease significantly in AUS/DSS and AUS/TAM with the distance from the source crater (Folco et al., 2010b, 2016) possibly owing to "bubble-stripping"

mechanism that was proposed to explain the loss of volatile in tektites and microtektites (Melosh and Artemieva, 2004).

No partially dissolved silica-rich lechatelierite-like inclusions, that are commonly observed in AUS/DSS and AUS/TAM microtektites (Glass, 1990; Folco et al., 2009; Folco et al., 2010b) were observed in the LKN spherules. Although their presence cannot be entirely excluded, they are at most extremely rare and may suggest that in LKN particles, possible target material was completely melted and digested during microtektite formation, consistently with more intense and/or longer heating compared to AUS/DSS and more particularly AUS/TAM microtektites.

Constant depletion of volatile and enrichment in refractory elements coupled with an extremely low vesicularity and likely absence of mineral inclusions suggest that LKN microtektites may represent the most vapor fractionated and intensely heated end-members of the Australasian strewn field discovered so far.

4.3. Accumulation mechanism of microtektites in the moraine

Knowing the accumulation mechanism of microtektites is critical to understanding whether they were deposited directly within the moraine at the time of formation or rather transported from another locality via the ice and/or wind. A recent study of the accumulation mechanisms of micrometeorites found within LKN moraine alongside the microtektites suggests that we cannot exclude the possibility that LKN microtektites were first deposited at a different locality before being windblown and trapped within the moraine (Suttle et al., 2015). The relatively high concentration of microtektites within the moraine (~200 particles/kg) rules against this hypothesis, as we would except such a scenario to quickly dilute the particles over large areas. Another possible accumulation mechanism is the recent release of microtektites in the moraine by sublimation of ice present directly underneath it. The age of the surface ice in the vicinity of LKN is unknown however, as well as the terrestrial age of meteorites recovered from the moraine. However, this would require ice at least as old as the microtektites, that is 0.8 Ma old considering that they are related to the Australasian strewn field. Such old ice surfaces have not been identified in the Transantarctic Mountains, which usually exhibit ice younger than 200–150 ka based on modeling of ice flow and exposure age of meteorites (Grinsted et al., 2003). Two scenarios are therefore envisioned: (1) direct infall of microtektites in the moraines at the time of their formation and (2) sublimation of earlier generations of ice that contained microtektites, before their preservation in the moraine. Similarly to Australasian microtektites recovered from Allan Hills (Folco et al., 2016), the lack of evidence of abrasion on any of the LKN microtektite suggests that a likely accumulation scenario is direct infall at the time of formation. The observation of abundant weathering pits on some LKN microtektites (Fig. 3b) suggests that they have been exposed to liquid water over long periods of time, similarly to V-type cosmic spherules (Van Ginneken et al., 2016), suggesting a long-lasting presence within the moraine, which is in agreement with a direct infall.

4.4. Implications

This new type of highly volatile-depleted microtektites puts new constraints on the formation and deposition of the Australasian strewn field. As mentioned earlier, LKN microtektites represent the southernmost extension of the Australasian strewn field. This strewn field is characterized by its tri-lobed shape (or butterfly pattern; Glass and Simonson, 2013). Larkman Nunatak microtektites thus currently represent the maximum extension of the main ejecta ray oriented toward SSE. This is in contrast with the two lateral lobes that extend WSW and ESE and have only been observed in deep sea cores in the Indian and Pacific Oceans (Glass and Simonson, 2013). Such an extension from the source crater further confirms that the impactor most likely came from a very oblique (i.e. <45°) NNW trajectory (e.g. Artemieva, 2008; Artemieva, 2013). Furthermore, cratering models suggest that ejecta thrown furthest from the source crater along ballistic trajectories were extracted nearest from the target area (Melosh, 1989). Assuming that distal ejecta are normally graded in terms of particle-sizes (e.g. Glass and Simonson, 2013), this would suggest that LKN microtektites, which are notably smaller than other Australasian microtektites (including AUS/TAM microtektites), currently represent the ejecta that was ejected closest to the target area (i.e. contact surface). Thus, they suffered the highest temperature regimes during their formation. This is consistent with their smaller size compared to other Australasian microtektites, high-temperature melts having smaller surface tensions that results in smaller particles (e.g. Artemieva et al., 2002). Higher temperature regimes are also consistent with the severe volatile depletion, the almost complete lack of vesicularity and mineral inclusions of the LKN microtektites. This, in turn, confirms the suggestion by Folco et al. (2010a, 2016) that volatile-content in microtektites decreases with increasing distance from the source crater (Fig. 9). In conclusion, the presence of Australasian microtektites as far as ~12,000 km from the hypothetical source crater give new constraints for future cratering models aiming at finding the actual crater location and/or studying the deposition of the Australasian strewn field (e.g. Artemieva et al., 2002).

Another important implication concerns the age of the newly discovered collection of micrometeorites that were found along with microtektites in LKN glacial moraine (Suttle et al., 2015; Van Ginneken et al., 2016). If we consider that LKN microtektites are part of the Australasian strewn field, that would imply that they were deposited in the moraine ~0.8 Ma ago. This would make the LKN micrometeorite collection as old as the TAM collection, which is consistent with the similar ranges of weathering states observed in both collection (Van Ginneken et al., 2016). Furthermore, the discovery of Australasian microtektites in sediments recovered from a low relief crest sampled at Allan Hills suggest that the East Antarctic Ice Sheet has been extremely stable in this area over the last ~1 Ma (Folco et al., 2016). Note that this is consistent with the discovery of numerous meteorites in blue ice fields close

to LKN (e.g., Corrigan et al., 2014). More importantly, this would imply that glacial moraines located close to nunataks in the Transantarctic Mountains are efficient sampling sites for micrometeorites and other extraterrestrial materials (e.g., meteoritic ablation debris). For example, similar areas could be surveyed to confirm the continental distribution of meteoritic ablation debris related to a large airburst event ~480 ka ago that were discovered in the TAM, Dome Fuji and Dome Concordia (Van Ginneken et al., 2010).

5. CONCLUSIONS

We report the discovery of microtektites in a glacial moraine near Larkman Nunatak. Geochemical evidence, both in term of major and trace elements, suggest that they may be related to the Australasian strewn field. This would further extend the Australasian strewn field by ~800 southward. Continuous depletion in volatiles and enrichment in refractory elements in Larkman Nunatak microtektites prolong the volatilization trend defined by Australasian microtektites, suggesting the former represent a new type of highly vapor fractionated microtektites. The fact that they are a new end-member to the volatilization trend is further supported by their very low vesicularity (i.e. almost complete loss of volatiles through boiling of the silicate melt) and absence of mineral inclusions (i.e. complete melting of target material due to extremely high and/or long temperature regimes). This discovery has strong implication for tektites/microtektites formation. Another important implication of the discovery of Australasian microtektites in the Larkman Nunatak area is that the East Antarctic Ice Sheet in this area may have been stable over the last ~1 Ma, confirming a similar observation the Allan Hills area, in the Transantarctic Mountains. Finally, old age and stability of glacial moraine at Larkman Nunatak suggest that such glacial moraines related to nunataks in the Transantarctic Mountains may be efficient sampling sites for infalling microscopic extraterrestrial matter, such as micrometeorites and meteoritic ablation debris.

ACKNOWLEDGMENT

This work was supported by the Science and Technology Facilities Council (STFC) [grant number: ST/J001260/1]. MVG thanks the Belgian Science Policy (program BRAIN.be) for present funding. C. Koeberl is acknowledged for editorial assistance. The manuscript benefited from constructive comments of Luigi Folco and an anonymous reviewer.

REFERENCES

Artemieva N., Pierazzo E. and Stöffler D. (2002) Numerical modeling of tektite origin in oblique impacts: implications to Ries-Moldavites strewn field. *Bull. Czech Geol. Survey* **77**, 303–311.

Artemieva N. (2008) High-velocity impact ejecta: tektites and Martian meteorites. In *Catastrophic Events Caused by Cosmic Objects* (eds. V. V. Adushkin and I. V. Nemchinov). Springer, Berlin, pp. 267–289.

Artemieva N. (2013) Numerical modeling of the Australasian tektite strewn field. *Lunar Planet. Sci.* **XXXXIV**, #1401 (abs.).

Corrigan C. M., Welzenbach L. C., Righter K., McBride K. M., McCoy T. J., Harvey R. P. and Satterwhite C. E. (2014) A statistical look at the U.S. Antarctic Meteorite Collection. *35 Seasons of U.S. Antarctic Meteorites (1976-2010): A Pictorial Guide To The Collection*. John Wiley & Sons.

Cassidy W. A., Glass B. P. and Heezen B. C. (1969) Physical and chemical properties of Australasian microtektites. *J. Geophys. Res.* **74**, 1008–1025.

Cordier C., Folco L. and Taylor S. (2011) Vestoid cosmic spherules from the South Pole Water Well and Transantarctic Mountains (Antarctica): A major and trace element study. *Geochim. Cosmochim. Acta* **75**, 1199–1215.

Cordier C., Suavet C., Folco L., Rochette P. and Sonzogni C. (2012) HED-like cosmic spherules from the Transantarctic Mountains, Antarctica: major and trace element abundances and oxygen isotopic compositions. *Geochim. Cosmochim. Act* **77**, 515–529.

Folco L., Rochette P., Perchiazzi N., D'Orazio M., Laurenzi M. and Tiepolo M. (2008) Microtektites from Victoria land transantarctic mountains. *Geology* **36**, 291–294.

Folco L., D'Orazio M., Tiepolo M., Tonarini S., Ottolini L., Perchiazzi N., Rochette P. and Glass B. P. (2009) Transantarctic Mountain microtektites. Geochemical affinity with Australasian microtektites. *Geochim. Cosmochim. Acta* **73**, 3694–3722.

Folco L., Glass B. P., D'Orazio M. and Rochette P. (2010a) A common volatilization trend in Transantarctic Mountain and Australasian microtektites: implications for their formation model and parent crater location. *Earth Planet. Sci. Lett.* **293**, 135–139.

Folco L., Perchiazzi N., D'Orazio M., Frezzotti M. L., Glass B. P. and Rochette P. (2010b) Shocked quartz and other mineral inclusions in Australasian microtektites. *Geology* **38**, 211–214.

Folco L., D'Orazio M., Gemelli M. and Rochette P. (2016) Stretching out the Australasian microtektite strewn field in Victoria Land Transantarctic Mountains. *Polar Sci.* **10**, 147–159.

Genge M. J., Engrand C., Gounelle M. and Taylor S. (2008) The classification of micrometeorites. *Meteorit. Planet. Sci.* **43**, 497–515.

Glass B. P. (1972) Bottle green microtektites. *J. Geophys. Res.* **35**, 7057–7064.

Glass B. P. (1990) Tektites and microtektites: key facts and inferences. *Tectonophysics* **171**, 393–404.

Glass B. P. and Pizzuto J. E. (1994) Geographic variation in Australasian microtektite concentrations: implications concerning the location and size of the source crater. *J. Geophys. Res.* **99**, 19075–19081.

Glass B. P., Huber H. and Koeberl C. (2004) Geochemistry of Cenozoic microtektites and clinopyroxene-bearing spherules. *Geochim. Cosmochim. Acta* **68**, 3971–4006.

Glass B. P. and Koeberl C. (2006) Australasian microtektites and associated impact ejecta in the South China Sea and the Middle Pleistocene supereruption of Toba. *Meteorit. Planet. Sci.* **41**, 305–326.

Glass B. P. and Simonson B. M. (2013) *Distal Impact Ejecta LayersA Record of Large Impacts in Sedimentary Deposits*. Springer, Heidelberg, New York, Dordrecht, London.

Grinsted A., Moore J., Spikes V. B. and Sinisalo A. (2003) Dating Antarctic blue ice areas using a novel ice flow model. *Geophys. Res. Lett. 30 CRY* **1–1**, 1–5.

Hinton R. W. (1999) NIST SRM 610, 611 and SRM 612, 613 multi-element glasses: constraints from element abundance ratios measured by microprobe techniques. *Geostand. Newslett.* **23**, 197–207.

Izett G. A. and Obradovich J. D. (1992) Laser-fusion $^{40}Ar/^{39}Ar$ ages of Australasian tektites. *Lunar Planet. Sci* **XXIII**, 593–594, abs.

Jackson S. (2008) LAMTRACE data reduction software for LA-ICP-MS Laser ablation ICP-MS in the Earth sciences: Current practices and outstanding issues: Mineralogical Association of Canada. *Short Course Series* **40**, 305–307.

Koeberl C. (1990) The geochemistry of tektites: an overview. *Tectonophysics* **171**, 405–422.

Koeberl C. (1994) Tektite origin by hypervelocity asteroidal or cometary impact: target rocks, source craters, and mechanisms. *Geol. Soc. Am. Spec. Pap.* **293**, 133–151.

Koeberl C., Bottomley R., Glass B. P. and Storzer D. (1997) Geochemistry and age of Ivory Coast tektites and microtektites. *Geochim. Cosmochim. Acta* **61**, 1745–1772.

Lee M.-Y. and Wei K.-Y. (2000) Australasian microtektites in the South China Sea and the West Philippine Sea: implications for age, size, and location of the impact crater. *Meteorit. Planet. Sci.* **35**, 1151–1155.

Lodders K. (2003) Solar system abundances and condensation temperatures of the elements. *Astrophys. J.* **591**, 1220–1247.

Ma P., Aggrey K., Tonzola C., Schnabel C., De Nicola P., Herzog G. F., Wasson J. T., Glass B. P., Brown L., Tera F., Middleton R. and Klein J. (2004) Beryllium-10 in Australasian tektites: constraints on the location of the source crater. *Geochim. Cosmochim. Acta* **68**, 3883–3896.

Melosh H. J. (1989) *Impact Cratering. A Geologic Process. Oxford Monographs on Geology and Geophysics No. 11*. Oxford University Press, Oxford, p. 245 (Clarendon Press New York).

Melosh H. J. and Artemieva N. (2004) How does tektite glass lose its water? *Lunar Planet. Sci.* **XXXV**, #1723, abs.

McDonough W. F. and Sun S. S. (1995) The composition of the Earth. *Chem. Geol.* **120**, 223–253.

Pouchou J. L. and Pichoir F. (1991) Quantitative analysis of homogeneous or stratified microvolumes applying the model "PAP". In *Electron Probe Quantification* (eds. K. F. J. Heinrich and D. E. Newbury). Plenum Press, New York, pp. 31–75.

Prasad M. S. and Sudhakar M. (1996) Impact microcraters on an Australasian microtektite. *Meteorit. Planet. Sci.* **31**, 46–49.

Prasad M. S. and Sudhakar M. (1999) Australasian minitektites discovered in the Indian Ocean. *Meteorit. Planet. Sci.* **34**, 179–184.

Prasad M. S., Mahale V. P. and Kodagali V. N. (2007) New sites of Australasian microtektites in the central Indian Ocean: implications for the location and size of source crater. *J. Geophys. Res.* **112**, E06007.

Suttle, M. D., Van Ginneken, M. and Genge M. J. (2015) Larkman Nunatak micrometeorites, a statistical study. In 78th Annual Meeting of the Meteoritical Society, #5063 (abs.).

Taylor S. R. and McLennan S. M. (1995) The geochemical evolution of the continental crust. *Rev. Geophys.* **32**, 241–265.

Taylor S., Herzog G. F. and Delaney J. S. (2007) Crumbs from the crust of Vesta: achondritic cosmic spherules from the South Pole water well. *Meteorit. Planet. Sci.* **42**, 223–233.

Van Ginneken M., Folco L., Perchiazzi N., Rochette P. and Bland P. A. (2010) Meteoritic ablation debris from the Transantarctic Mountains: Evidence for a Tunguska-like impact over Antarctica ca. 480 ka ago. *Earth Planet. Sci. Lett.* **293**, 104–113.

Van Ginneken M., Genge M. J., Folco L. and Harvey R. P. (2016) The weathering of micrometeorites from the Transantarctic Mountains. *Geochim. Cosmochim. Acta* **179**, 1–31.

Wasson J. T., Ouyang X. and Stovall W. K. (1990) Uranium volatilization during tektite formation. *Meteoritics* **25**, 419, abs.

Associate editor: Christian Koeberl